J Mater Sci (2007) 42:8438–8446
DOI 10.1007/s10853-007-1776-6

Effects of milling time and calcination condition on phase formation and particle size of lead zirconate nanopowders prepared by vibro-milling

O. Khamman · T. Sarakonsri · A. Rujiwatra · Y. Laosiritaworn · R. Yimnirun · S. Ananta

Received: 7 November 2006 / Accepted: 13 April 2007 / Published online: 28 June 2007

Abstract Effect of calcination conditions on phase formation and particle size of lead zirconate ($PbZrO_3$) powders synthesized by a solid-state reaction with different vibro-milling times was investigated. A combination of the milling time and calcination conditions was found to have a pronounced effect on both the phase formation and particle size of the calcined $PbZrO_3$ powders. The calcination temperature for the formation of single-phase perovskite lead zirconate was lower when longer milling times were applied. The optimal combination of the milling time and calcination condition for the production of the smallest nanosized (~28 nm) high purity $PbZrO_3$ powders is 35 h and 750 °C for 4 h with heating/cooling rates of 30 °C/min, respectively.

Introduction

Lead zirconate, $PbZrO_3$ or PZ, is one of the widely investigated antiferroelectric materials with a perovskite structure. The unique properties such as high transition temperature (~230 °C), free of remanant polarization and double hysteresis behaviour make it an interesting candidate for many applications especially for energy storage, low-loss linear capacitors, microelectronics and actuators [1, 2]. There has been a great deal of interest in the preparation of single-phase PZ powders as well as in the sintering and electrical properties of PZ-based ceramics [2, 3]. To fabricate them, a fine powder of perovskite phase with the minimized degree of particle agglomeration is needed as starting material in order to achieve a dense and uniform microstructure at the sintering temperature [1–3]. Some typical processes to synthesize perovskite lead-based powders are the microemulsion [4], the sol–gel technique [5], the co-precipitation [6], the hydrothermal reaction [7], mechanical activation [8, 9], and the solid-state reaction or mixed oxides [10].

Recently, ultrafine powders (<100 nm in diameter) are promising starting materials in the fabrication of advanced nanoceramics [2, 3]. However, the evolution of a method to produce nano-sized powders of precise stoichiometry and desired properties is complex, depending on a number of variables such as starting materials, processing history, temperature, etc. The advantage of using a solid-state reaction method via mechanical milling for preparation of nano-sized powders lies in its ability to produce mass quantities of powder in the solid state using simple equipment and low cost starting precursors [11, 12]. Although our earlier work has been done in the preparation of PZ powders via a vibro-milling technique [13], a detailed study considering the role of both milling times and firing conditions on the preparation of PZ nanopowders has not been reported yet.

Therefore, the present work has been undertaken to investigate the effects of vibro-milling time together with calcination conditions on phase formation and particle size of lead zirconate powders synthesized by solid-state reaction method. The powder characteristics of the vibro-milling derived $PbZrO_3$ have also been thoroughly investigated.

O. Khamman · Y. Laosiritaworn · R. Yimnirun · S. Ananta (✉)
Department of Physics, Faculty of Science, Chiang Mai University, and NANOTEC Center of Excellence at Chiang Mai University, Chiang Mai 50200, Thailand
e-mail: suponananta@yahoo.com

T. Sarakonsri · A. Rujiwatra
Department of Chemistry, Faculty of Science, Chiang Mai University, Chiang Mai 50200, Thailand

Experimental procedure

The raw materials used were commercially available lead oxide, PbO (JCPDS file number 77-1971) and zirconium oxide, ZrO_2 (JCPDS file number 37–1484) (Fluka, >99% purity). The two oxide powders exhibited an average particle size in the range of 3.0–5.0 μm. $PbZrO_3$ powder was synthesized by the solid-state reaction of these raw materials, in analogous with other similar lead-based perovskites as described in our previous works [12, 14]. A McCrone vibro-milling technique [11, 12] was employed for preparing the stoichiometric $PbZrO_3$ powders. In order to improve the reactivity of the constituents, the milling process was carried out for various milling times ranging from 15 to 35 h (instead of 30 min [13]) with corundum media in isopropanol. After drying at 120 °C for 2 h, various calcination conditions, i.e. temperature ranging from 550 to 800 °C, dwell times ranging from 1 to 6 h and heating/cooling rates ranging from 10 to 30 °C/min, were applied (the powders were calcined in air inside a closed alumina crucible) in order to investigate the formation of $PbZrO_3$ [13].

All powders were subsequently examined by room temperature X-ray diffraction (XRD; Siemens-D500 diffractometer) using Ni-filtered CuK_α radiation, to identify the phases formed, optimum milling time and firing conditions for the production of single-phase $PbZrO_3$ powders. The crystalline lattice constants and average particle size were also estimated from the diffraction peak (240) of the perovskite pattern using Scherrer equation [15]. The particle size distributions of the powders were determined by laser diffraction technique (DIAS 1640 laser diffraction spectrometer) with the particle sizes and morphologies of the powders observed by scanning electron microscopy (JEOL JSM-840A SEM). The structures and chemical compositions of the phases formed were elucidated by transmission electron microscopy (CM 20 TEM/STEM operated at 200 keV) and an energy-dispersive X-ray (EDX) analyzer with an ultra-thin window. EDX spectra were quantified with the virtual standard peaks supplied with the Oxford Instrument eXL software. Powder samples were dispersed in solvent and deposited by pipette on to 3 mm holey copper grids for observation by TEM. In addition, attempt was made to evaluate the crystal structures of the observed compositions/phases by correcting the XRD and TEM diffraction data.

Results and discussion

Powder XRD patterns of the calcined samples after different milling times are given in Figs. 1–3, with the corresponding JCPDS patterns. As shown in Fig. 1, for the uncalcined powder subjected to 15 h of vibro-milling and the powders calcined at 550 °C, only X-ray peaks of precursors PbO (●) and ZrO_2 (○) are present, indicating that no reaction was yet triggered during the vibro-milling or low firing processes, in agreement with literatures [13, 16]. However, it is seen that crystalline phase of the perovskite $PbZrO_3$ (▼) was found as separated phase in the powders calcined at 600 °C, and became the predominant phase in the powders calcined at 700 °C. Further calcination at 800 °C with dwell time of 1 h does not result in very much increase in the amount of $PbZrO_3$ whereas the traces of

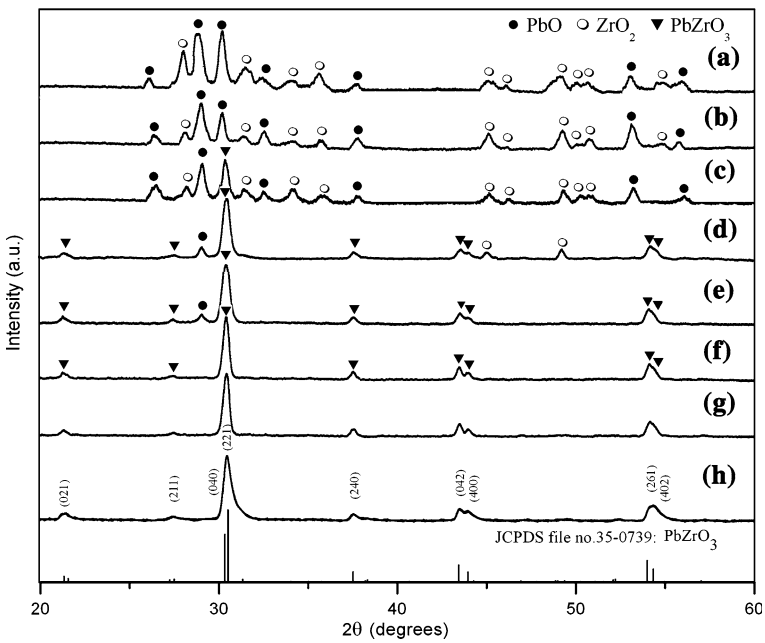

Fig. 1 XRD patterns of $PbZrO_3$ powders milled for 15 h (**a**) uncalcined, and calcined for 2 h with heating/cooling rates of 10 °C/min at (**b**) 550 (**c**) 600 and (**d**) 700 °C, at 800 °C for (**e**) 1 and (**f**) 2 h, and at 800 °C for 2 h with heating/cooling rates of (**g**) 20 and (**h**) 30 °C/min

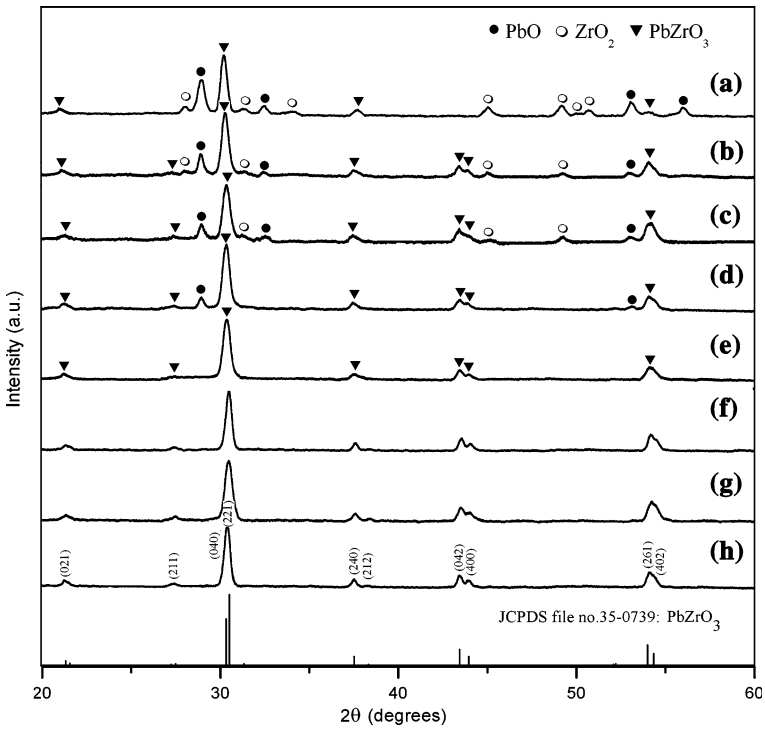

Fig. 2 XRD patterns of $PbZrO_3$ powders milled for 25 h and calcined for 2 h with heating/cooling rates of 10 °C/min at (**a**) 600 (**b**) 700 and (**c**) 750 °C, at 750 °C for (**d**) 5 and (**e**) 6 h, and at 750 °C for 6 h with heating/cooling rates of (**f**) 20 and (**g**) 30 °C/min, and (**h**) at 800 °C for 1 h with heating/cooling rates of 30 °C/min

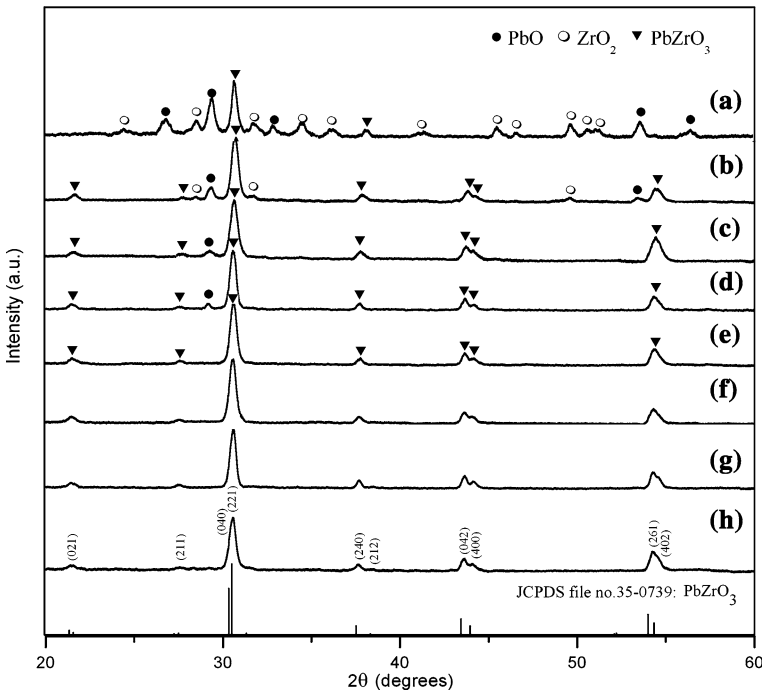

Fig. 3 XRD patterns of $PbZrO_3$ powders milled for 35 h and calcined for 2 h with heating/cooling rates of 10 °C/min at (**a**) 600 (**b**) 700 and (**c**) 750 °C, at 750 °C for (**d**) 3 and (**e**) 4 h, and at 750 °C for 4 h with heating/cooling rates of (**f**) 20 and (**g**) 30 °C/min, and (**h**) at 800 °C for 1 h with heating/cooling rates of 30 °C/min

unreacted PbO could not be completely eliminated. This could be attributed to the poor reactivity of lead and zirconium species [10, 13]. However, it should be noted that after calcination at 800 °C for 2 h (Fig. 1f), the single phase of perovskite $PbZrO_3$ (yield of 100% within the limitations of the XRD technique) was obtained. In general, the strongest reflections apparent in the majority of these XRD patterns indicate the formation of $PbZrO_3$. These can be matched with JCPDS file number 35-0739 for the orthorhombic phase, in space group *P2cb* (no. 32) with cell parameters $a = 823.1$ pm $b = 1177$ pm, and $c = 588.1$ pm [17], consistent with other works [7, 13, 16].

For 15 h of milling, the optimum calcination temperature for the formation of a high purity $PbZrO_3$ phase was found to be about 800 °C.

To further study the phase development with increasing milling times, an attempt was also made to calcine mixed powders milled at 25 h and 35 h under various conditions as shown in Figs. 2 and 3, respectively. In this connection, it is seen that by varying the calcination temperatures and dwell times, the minimum firing temperature or dwell time for the single perovskite phase formation of each milling batch is decreased with increasing milling time (Figs. 1–3), in good agreement with other perovskite systems [12, 14, 18]. The main reason for this behavior is that a complete solid-state reaction probably takes place more easily when the particle size is milled down by accelerating an atomic diffusion mechanism to meet the suitable level of homogeneity mixing. It is thought that the reduction in the particle sizes significantly reduces heat diffusion limitations. It is therefore believed that the solid-state reaction to form perovskite $PbZrO_3$ phase occurs at lower temperatures or shorter dwell times with decreasing the particle size of the oxide powders [11, 12].

As expected, there is evidence that, even for a wide range of calcination conditions, single-phase $PbZrO_3$ cannot easily be produced, in agreement with literatures [13, 16]. In the work reported here, evidence for the minor phase of PbO which coexists with the parent phase of $PbZrO_3$ is found after calcination at temperature 600–750 °C, in agreement with literature [13, 16]. This second phase has an orthorhombic structure with cell parameters $a = 589.3$ pm, $b = 549.0$ pm and $c = 475.2$ pm (JCPDS file number 77-1971) [19]. This observation could be attributed mainly to the poor reactivity of lead and zirconium species [13] and also the limited mixing capability of the mechanical method [11, 12]. A noticeable difference is noted when employing the milling time longer than 15 h (Figs. 2, 3), since an essentially monophasic $PbZrO_3$ of perovskite structure was obtained at 800 °C for 1 h or 750 °C for 6 h (or 4 h) for the milling time of 25 h (or 35 h). This was apparently a consequence of the enhancement in crystallinity of the perovskite phase with increasing degree of mixing and dwell time, in good agreement with other works [12, 18].

In the present study, an attempt was also made to calcine the powders with different milling times under various heating/cooling rates (Figs. 1–3). In this connection, it is shown that the yield of $PbZrO_3$ phase did not vary significantly with different heating/cooling rates ranging from 10 to 30 °C/min, in good agreement with the early observation for the $PbZrO_3$ powders subjected to 0.5 h of vibro-milling times [13]. The variation of calculated crystallite size of the $PbZrO_3$ powders milled for different times with the calcination conditions is given in Table 1. In general, it is seen that the calculated crystallite size of $PbZrO_3$ decreases with increasing heating/cooling rates for all different milling times. These values indicate that the particle size affects the evolution of crystallinity of the phase formed by prolong milling treatment. It should be noted that no evidences of the introduction of impurity due to wear debris from the selected milling process was observed in all calcined powders, indicating the effectiveness of the vibro-milling technique for the production of high purity $PbZrO_3$ nanopowders. Moreover, it has been observed that with increasing milling time, all diffraction lines broaden, e.g. (261) and (402) peaks, which are an indication of a continuous decrease in particle size and of the introduction of lattice strain (Fig. 4) [15].

For $PbZrO_3$ powders, the longer the milling time, the finer is the particle size (Fig. 4 and Table 1). Also the relative intensities of the Bragg peaks and the calculated

Table 1 Effect of calcination conditions on the variation of particle size of $PbZrO_3$ powders milled for different times

Milling time (h)	Calcination condition *T/D/R* (°C:h:°C/min)	XRD (nm, ± 2.0)				SEM (nm, ± 10)		Laser scattering (nm, ± 200)	
		A	*a*	*b*	*c*	*D*	*P*	*D*	*P*
15	800/2/10	60.44	0.8255	1.1679	0.5873	306	65–522	720	40–2000
15	800/2/30	60.41	0.8257	1.1682	0.5875	280	53–692	700	35–2000
25	800/1/10	38.38	0.8242	1.1723	0.5877	235	36–415	190	35–800
25	800/1/30	35.11	0.8239	1.172	0.5875	223	31–400	170	35–750
35	750/4/10	32.45	0.8227	1.1672	0.587	160	39–420	1600	10–4500
35	750/4/20	30.94	0.8231	1.1769	0.5868	152	36–390	1580	10–5000
35	750/4/30	27.5	0.8235	1.1729	0.5854	121	31–228	1570	10–6000

A = Crystallite size

a, b, c = Lattice parameters

D = Average particle size

P = Particle size range or distribution

T/D/R = Calcination temperature, dwell time and heating/cooling rates

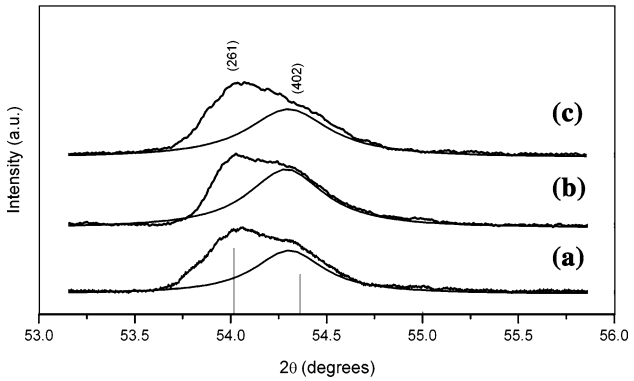

Fig. 4 Enlarged zone of XRD patterns showing (261)/(402) peaks broadening of $PbZrO_3$ powders milled for (**a**) 15 h (Fig. 1(h)), (**b**) 25 h (Fig. 2(h)) and (**c**) 35 h (Fig. 3(g))

crystallite size for the powders tend to decrease with the increase of milling time. However, it is well documented that, as Scherer's analysis provides only a measurement of the extension of the coherently diffracting domains, the particle sizes estimated by this method can be significantly under estimated [15, 18]. In addition to strain, factors such as dislocations, stacking faults, heterogeneities in composition and instrumental broadening can contribute to peak broadening, making it almost impossible to extract a reliable particle size solely from XRD [15, 20].

In this connection, a combination between scanning electron microscopy and laser diffraction techniques was also employed for particle size measurement (Table 1). The morphological evolution and particle size distribution during various calcination conditions of $PbZrO_3$ powders milled with different times were investigated as shown in Fig. 5. At first sight, the morphological characteristic of $PbZrO_3$ powders with various milling times is similar for all cases. In general, the particles are agglomerated and basically irregular in shape, with a substantial variation in particle sizes and size distribution, particularly in powders subjected to prolong milling times. Fracture is considered to be the major mechanism at long milling times. The powders consist of primary particles of nanometers in size and the agglomerates measured ~0.75–6.00 μm. In addition to the primary particles, the powders have another kind

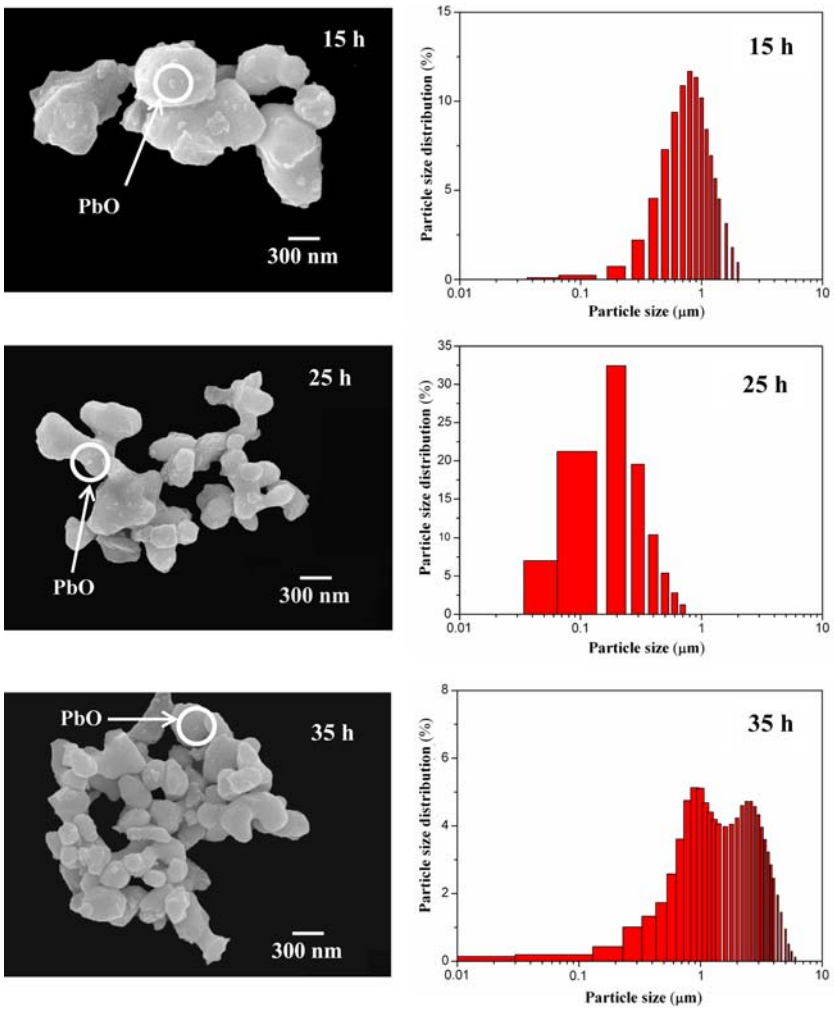

Fig. 5 SEM micrographs and particle size distributions of $PbZrO_3$ powders milled for (**a**) 15 h (Fig. 1(h)), (**b**) 25 h (Fig. 2(h)) and (**c**) 35 h (Fig. 3(g))

of very fine particle (brighter particles) with diameter of about 30 nm. However, as unidentified by the XRD technique, a combination of SEM and EDX techniques has demonstrated that unreacted PbO phases (Fig. 6b) (circled in the micrographs in Fig. 5) exist in neighbouring to the parent $PbZrO_3$ phase. In general, EDX analysis using a 20 nm probe on a large number of particles of the calcined powders confirmed the parent composition to be $PbZrO_3$ (Fig. 6a). As listed in Table 1, the comparison of XRD crystallite size with SEM apparent crystallite size indicates

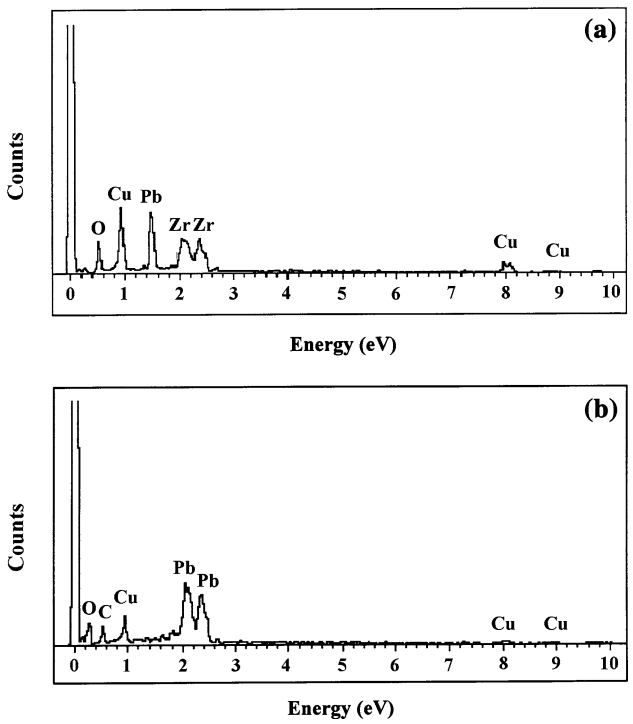

Fig. 6 EDX analysis of (**a**) the major phase $PbZrO_3$ and (**b**) the minor phase PbO (some signals of C and Cu come from coated electrodes and sample stubs, respectively)

that the nanoparticles of PZ obtained in this study are indeed polycrystalline, not single-domain single crystalline as in the case of $PbTiO_3$ nanoparticles [21]. This clearly suggests the possibility of introducing excess crystalline defects through vibro-milling.

The effect of milling time on particle size distribution was found to be significant, as shown in Fig. 5. After milling times of 15 and 25 h, the powders have a similar particle size distribution. They exhibit a single peak covering the size ranging from 35 to 2000 nm. However, upon further increase of milling time up to 35 h, a bimodal distribution curve with peak broadening between 10 and 6000 nm is observed. This behavior is believed to arise mainly from particle agglomeration, consistent with SEM result where the strong interparticle bond within each aggregate is evident by the formation of a well-established necking between neighbouring particles (Fig. 5). This observation could be attributed to the mechanism of surface energy reduction of the ultrafine powders, i.e. the smaller the powder the higher the specific surface area [22]. However, it should also be noticed in Fig. 5 that there is a possible necking is observed in long milling time, i.e. 25 h. This necking could be a result of local melting caused by vibro-milling technique. This statement is also supported by the large agglomeration at longer milling time, i.e. 35 h, detected by laser diffraction. Nonetheless, even with the possibility of thermally induced necking, the nanosized particles could still be obtained with the vibro-milling technique, as seen in Fig. 5.

Bright field TEM images of the calcined $PbZrO_3$ powders derived from milling time of 35 and 25 h are shown in Figs. 7a and 8a, respectively. By employing a combination of both selected area electron diffraction (SAED) and crystallographic analysis, the major phase of orthorhombic $PbZrO_3$ (Figs. 7b, 8b) was identified, in good agreement with the XRD results. It is interesting to note that limited evidence for the presence of the unreacted

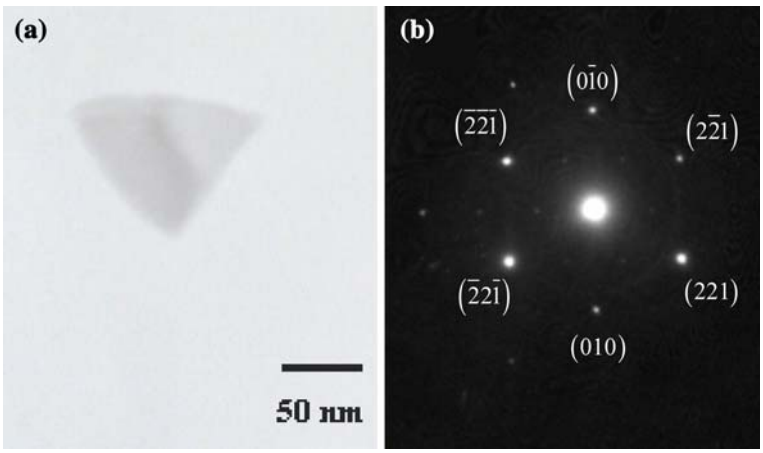

Fig. 7 (**a**) TEM micrograph and (**b**) SAED pattern ([13$\bar{1}$] zone axis) of $PbZrO_3$ powders milled for 35 h (Fig. 3(g))

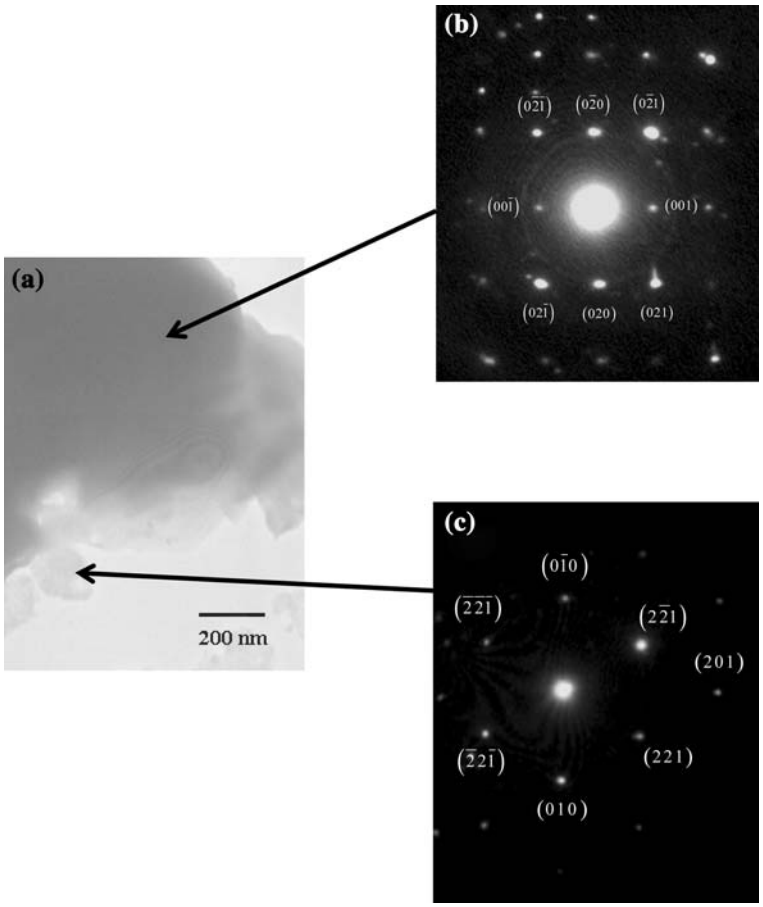

Fig. 8 (**a**) TEM micrograph of $PbZrO_3$ powders milled for 25 h (Fig. 2(h)) and SAED pattern of (b) major phase $PbZrO_3$ ([$\bar{1}$02] zone axis) and (**c**) minor phase PbO ([$\bar{2}$00] zone axis)

precursor PbO (Fig. 8c), in good agreement with the SEM results, was also found in the TEM-SAED investigation, even though this could not be detected by XRD. It is, therefore, intriguing to note the advantage of a combination between TEM-SAED and SEM-EDX techniques, which lies in its ability to reveal microstructural features often missed by the XRD method which requires at least 5 wt% of the component [7, 15].

The experimental work carried out here suggests that the optimal combination of the milling time and calcination condition for the production of the smallest nanosized high purity $PbZrO_3$ powders is 35 h and 750 °C for 4 h with heating/cooling rates of 30 °C/min, respectively. Moreover, the employed heating/cooling rates for $PbZrO_3$ powders observed in this work are also faster than those reported earlier [13, 16]. This investigation indicates a strong relationship between the vibro-milling process, the calcination condition and the yield of $PbZrO_3$ nanopowders.

Furthermore, it is a well-established fact that ferroelectric nanoparticles undergo what is called a finite-size effect [21, 23]. Namely, at a certain particle size called the critical size, the high-temperature paraelectric phase is stabilized at room temperature. Prior to reaching that size, the lattice parameters as well as the paraelectric–ferroelectric phase transition temperature changes. However, there has been much controversy concerning the critical size at room temperature. The critical crystallite size has been reported to range between 25 and 200 nm [21, 23–29]. In particular, earlier report has shown that the critical crystallite size in PZ is approximately 100 nm [23, 24]. In view of this connection, an attempt has been made to determine the critical crystallite size for the PZ nanoparticles produced in this study. As shown in Fig. 9, the critical crystallite size for the PZ seems to be around 30–35 nm. It should also be noticed that there is an increase in lattice parameters and unit-cell volume at smaller particle size, which could be attributed to crystallite aggregation, as reported earlier in $BaTiO_3$ [25] and also in good agreement with SEM results (Fig. 5) which show aggregated clusters. It is also to be noted the critical crystallite size obtained in this study is significantly lower than previously reported values [23, 24]. This is mainly due to the range of the particle size used for the critical size determination is limited to 27–60 nm, as compared to 30–250 nm in previous studies [23–29]. Therefore, more accurate value can be obtained with wider range of particle sizes.

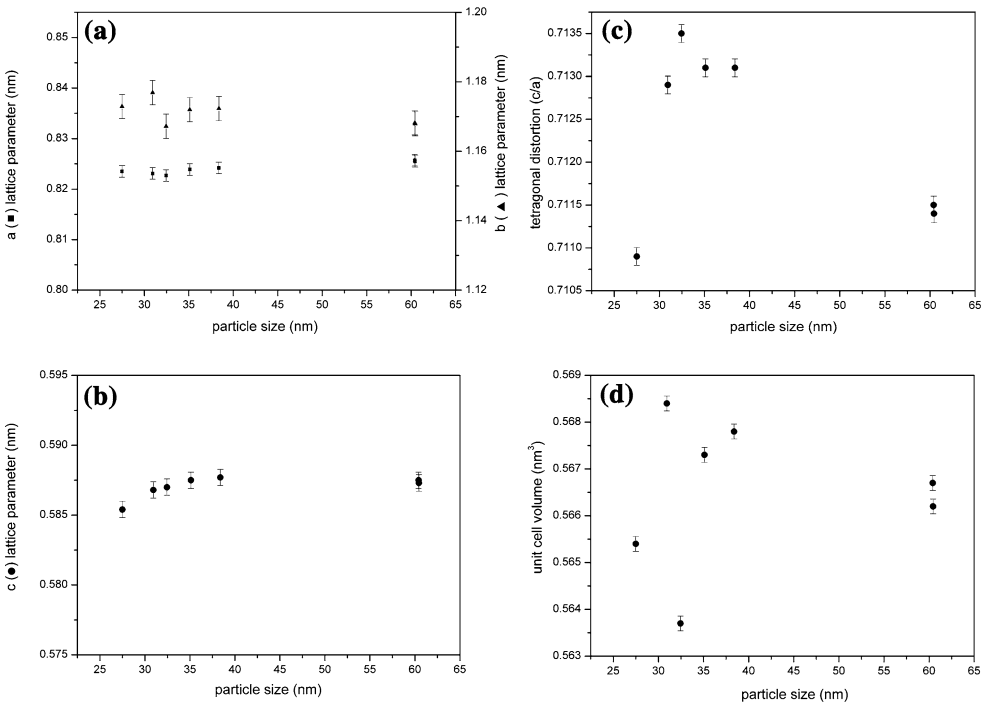

Fig. 9 Values of (**a**) a (■) and b (▲) lattice parameters, (**b**) c (●) lattice parameter, (**c**) tetragonal distortion (c/a), and (**d**) unit cell volume as a function of the particle size (XRD crystallite size) in single-phase $PbZrO_3$ powders

Conclusions

This work demonstrated that by applying an appropriate choice of the vibro-milling time, calcination temperature and dwell time, mass quantities of a high purity lead zirconate nanopowders can be successfully produced by a simple solid-state mixed oxide synthetic route without the use of high purity starting precursors. A combination of the milling time and calcination conditions was found to have a pronounced effect on both the phase formation and particle size of the calcined $PbZrO_3$ powders. The calcination temperature for the formation of single-phase perovskite lead zirconate was lower when longer milling times were applied. The optimal combination of the milling time and calcination condition for the production of the smallest nanosized (~28 nm) high purity $PbZrO_3$ powders is 35 h and 750 °C for 4 h with heating/cooling rates of 30 °C/min, respectively.

Acknowledgment This work was supported by the National Nanotechnology Center (NANOTEC), NSTDA, Ministry of Science and Technology, the Thailand Research Fund (TRF), the Commission on Higher Education (CHE), Faculty of Science, and the Graduate School of Chiang Mai University.

References

1. Jaffe B, Cook WR, Jaffe H (1971) Piezoelectric ceramics Academic Press, New York
2. Moulson AJ, Herbert JM (2003) Electroceramics, 2nd edn. Wiley, Chichester
3. Haertling GH (1999) J Am Ceram Soc 82:797
4. Rao YS, Sunandana CS (1992) J Mater Sci Lett 11:595
5. Ibrahim DM, Hennicke HW (1981) Trans J Br Ceram Soc 80:18
6. Oren EE, Taspinar E, Tas AC (1997) J Am Ceram Soc 80:2714
7. Rujiwatra A, Tapala S, Luachan S, Khamman O, Ananta S (2006) Mater Lett 60:2893
8. Lanagan MT, Kim JH, Jang S, Newnham RE (1988) J Am Ceram Soc 71:311
9. Lee SE, Xue JM, Wan DM, Wang J (1999) Acta Mater 47: 2633
10. Xue JM, Wan DM, Lee SE, Wang J (1999) J Am Ceram Soc 82:1687
11. Ngamjarurojana A, Khamman O, Yimnirun R, Ananta S (2006) Mater Lett 60:2867
12. Wongmaneerung R, Yimnirun R, Ananta S (2006) Mater Lett 60:1447
13. Chaisan W, Khamman O, Yimnirun R, Ananta S J Mater Sci (to be published)
14. Ananta S, Thomas NW (1999) J Eur Ceram Soc 19:155
15. Klug H, Alexander L (1974) X-Ray diffraction procedures for polycrystalline and amorphous materials, 2nd edn. Wiley, New York
16. Puchmark C, Rujijanagul G, Jiansirisomboon S, Tunkasiri T (2004) Ferroelectric Lett 31:1
17. Powder Diffraction File No. 35–0739. International Centre for Diffraction Data, Newtown Square, PA, 2000
18. Wongmaneerung R, Yimnirun R, Ananta S (2006) Mater Lett 60:2666
19. Revesz A, Ungar T, Borbely A, Lendvai J (1996) Nanostruct Mater 7:779
20. Reed JS (1995) Principles of ceramic processing, 2nd edn. Wiley, New York
21. Chattopadhyay S, Ayyub P, Palkar VR, Multani M (1995) Phys Rev B 52:13177
22. Powder Diffraction File No. 77-1971. International Centre for Diffraction Data, Newtown Square, PA, 2000

23. Chattopadhyay S, Ayyub P, Palkar VR, Gurjar AV, Wankar RM, Multani M (1997) J Phys: Condens Matter 9:8135
24. Chattopadhyay S (1997) NanoStructured Mater 9:551
25. Leonard MR, Safari A (1996) IEEE ISAF 2:1003
26. Uchino K, Sadanaga E, Hirose T (1989) J Am Ceram Soc 72:1555
27. Begg BD, Vance ER, Nowotny J (1994) J Am Ceram Soc 77:3186
28. Saegusa K, Rhine WE, Bowen HK (1993) J Am Ceram Soc 76:1505
29. Li X, Shih WH (1997) J Am Ceram Soc 80:2844